UCRL-85102
PREPRINT

CALIBRATION OF A NEUTRON LOG IN PARTIALLY SATURATED MEDIA, PART II: ERROR ANALYSIS*

J. R Hearst, P. W. Kasameyer, and L. A. Dreiling
Lawrence Livermore National Laboratory
Livermore, California

ABSTRACT

We have studied four sources of error (uncertainty) in water content obtained from neutron logs calibrated in partially saturated media for holes up to 3 m. For this calibration we built a special facility and developed an algorithm for a commercial epithermal neutron log that obtains water content from count rate, bulk density, and gap between the neutron sonde and the borehole wall. In our study we found errors in the facility itself: finite length of the cells making up the facility, inhomogeneous and nonrepresentative material within the cells, gaps between the cells, inappropriate borehole shape, and approximation of a large borehole by a flat face. The algorithm contained errors due to the calibration and lack of fit, while the field measurements included uncertainties in the count rate (caused by statistics and a short time constant), gap, and density. Finally, there can be inhomogeneity in the material surrounding the borehole. Under normal field conditions the hole-size-corrected water content obtained from such neutron logs can have an uncertainty as large as 15% of its value. Primary causes are uncertainty in gap (correctable by measuring at both ends of the sonde), uncertainty in count (reducible by averaging over depth), and lack of fit. We intend to (1) increase the thickness of the sonde's shielding to

---

*Work performed under the auspices of the U.S. Department of Energy by the Lawrence Livermore National Laboratory under contract No. W-7405-ENG-48.

eliminate hole-size effect as well as (2) correct for uncertainties in gap and count. Then we believe we can reduce the uncertainty in the hydrogen index to the larger of 0.02 or 8% of its value, most of which is systematic.

INTRODUCTION

To meet our needs for determining the hydrogen index in support of the Lawrence Livermore National Laboratory (LLNL) Nuclear Testing Program at the Nevada Test Site (NTS), we have calibrated an epithermal neutron log for partially saturated media and large holes. Epithermal neutron logs are used because compensated thermal neutron logs are marginally useful (Allen et al., 1972) in the presence of boron and gadolinium. These two thermal neutron absorbers, boron and gadolinium, are unusually common at NTS; their quantity varies with position (Diment, 1959).

Careful examination of the calibration procedure and use of the logging sonde in the field has resulted in a set of estimates of systematic and random errors in water content. Many of these sources of error are common to all nuclear-log calibration procedures but have not, to our knowledge, been addressed in the literature. Therefore, our results should be of interest to those involved in this field.

We have performed our own calibration of a service-company logging system because we need to be able to predict the influence of formation water content on the effects of underground nuclear explosions. Therefore, we need to estimate total water content--bound as well as free. If we consider water content to be represented by the hydrogen index I_H (defined as hydrogen per unit volume compared to that in fresh water), then we need to know I_H within 0.02 or 10% of its value (whichever is larger).

Also, our holes and formations are unusual. Most of the holes we log are large--from 1.5 to 3 m in diameter--and dry. The hole walls are often quite rough, with severe washouts.

Because porosity is often very high and water saturations very low, conventional neutron-log calibrations, made in saturated media, require us to make large corrections for density (Segisman and Liu, 1971). In addition, there are no service-company calibrations for 1- or 2-m diam holes, and those

used for 30- to 50-cm diam dry holes result in implausible water contents when standard logs are run in our holes.

To meet our special needs and conditions, we built our own calibration facility at NTS (Hearst, 1979). Called the Hydrogen Content Test Facility (HCTF), the primary purpose of the calibration structure was to simulate large (1.5- to 3-m diam), dry holes. Furthermore, it was designed to have a range of bulk density and water content that spanned the range expected to be of interest to LLNL programs. We used such a range of densities because (1) the calculated density correction to the service-company calibrations might not apply to our case, and (2) there are no published measurements of the effect of density. Construction of this facility allowed us to introduce gaps between the logging sonde and the borehole wall; it also permitted us to perform some crude small-hole (30-cm diam) calibrations. Figure 1 is a photograph of the HCTF.

During the past two years we have expanded and improved this facility, using it to calibrate two different sondes. The first sonde was a standard service-company epithermal-neutron sonde with shielding added to attempt to eliminate the effect of the borehole size. The second was a sonde designed especially for our large boreholes.

We have fitted new interpolation algorithms depending on bulk density, water content, and gap to the data from each of these sondes. Each sonde was calibrated in water-filled and dry boreholes, and the standard sonde was calibrated in both large and small holes. We used an algorithm having few enough parameters to permit some statistical analysis of the accuracy of estimation of water content between the calibration points. This report is an account of the calibration and error analysis in the improved HCTF.

THE IMPROVED CALIBRATION FACILITY

The current facility is made up of 12 sets of cells arranged in parallelepipeds, each set consisting of 15 aluminum cells. Each set contains a different combination of water content and density, as shown in Table 1.

Figure 2 shows a sketch of the layout of three sets of the cells. In this illustration we demonstrate how two sizes of dry holes can be simulated.

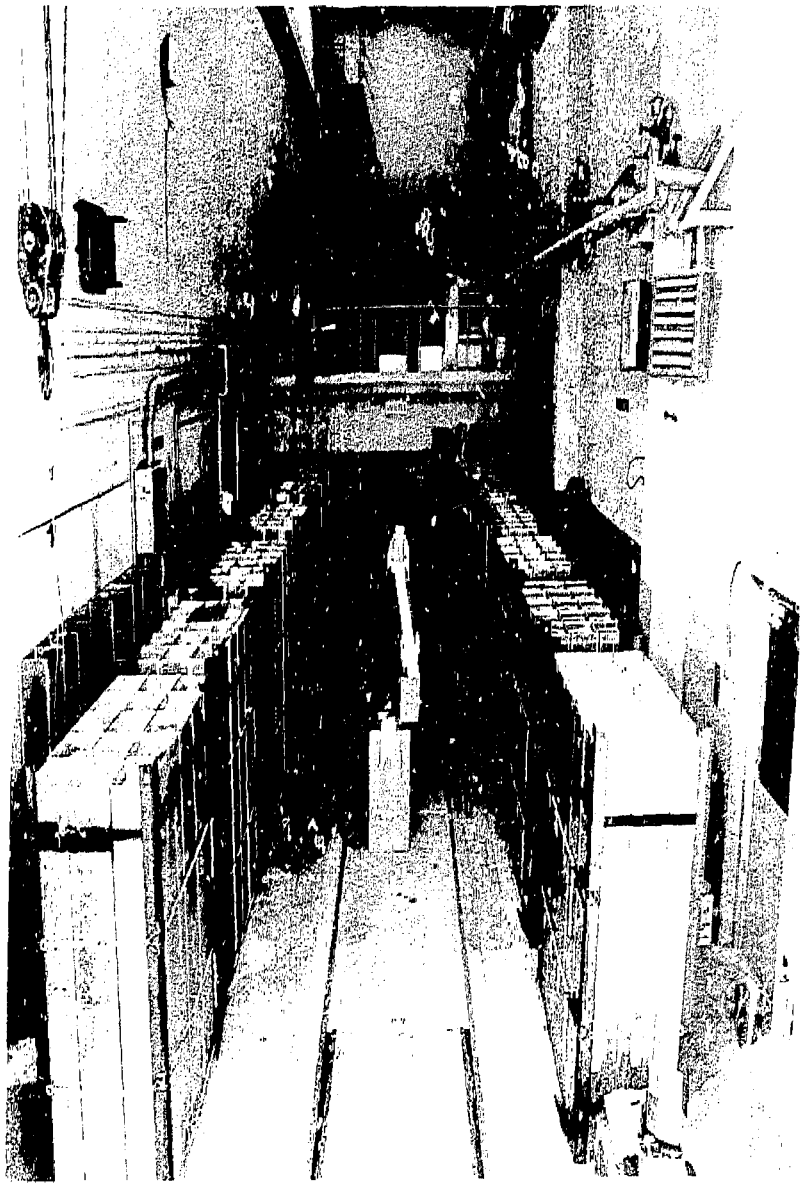

FIG. 1. The LLNL Hydrogen Content Test Facility at the Nevada Test Site. Cell sets are on either side of center aisle. (Workbench not present during use of the facility.)

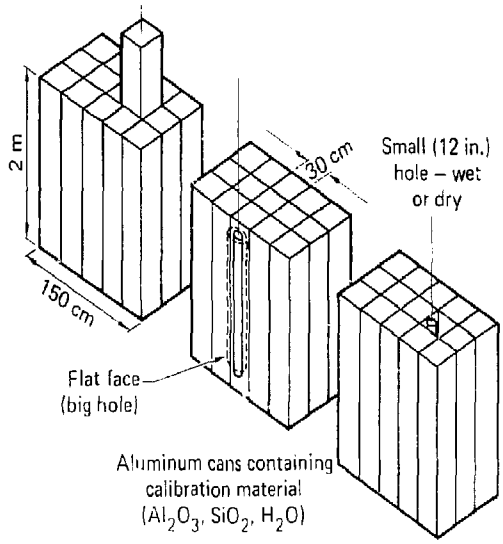

FIG. 2. Sketch of three of the 12 parallelepipeds, which were designed to calibrate neutron logs.

A sonde can be placed on the face of the center cell of a set to approximate a large hole or inside the space left by removing the inner cell to approximate a small hole. The face of a set of cells is intended to simulate an infinite-diam hole. We expected that there would be enough shielding on the sonde to prevent neutrons from entering the sonde anywhere but at its front face, making this arrangement a good simulation of our large-diam holes. Figure 3 is a photograph of an actual sonde (with no shield) in place on a cell face.

It is also possible to simulate two sizes of wet holes at the HCTF. We approximated a large, water-filled hole by cutting a piece of 1.3-m diam casing in half longitudinally and welding a plate across the diam. A thin, aluminum plate was placed across a slot at the center of this latter plate. The assembly was situated so the aluminum plate bore against the center of the face of a set of cells. This half-piece of casing was then filled with water and used to simulate the large water-filled hole. For a small, water-filled hole we replaced one of the center cells with a water-filled cell and put the sonde in that cell, forced against one wall.

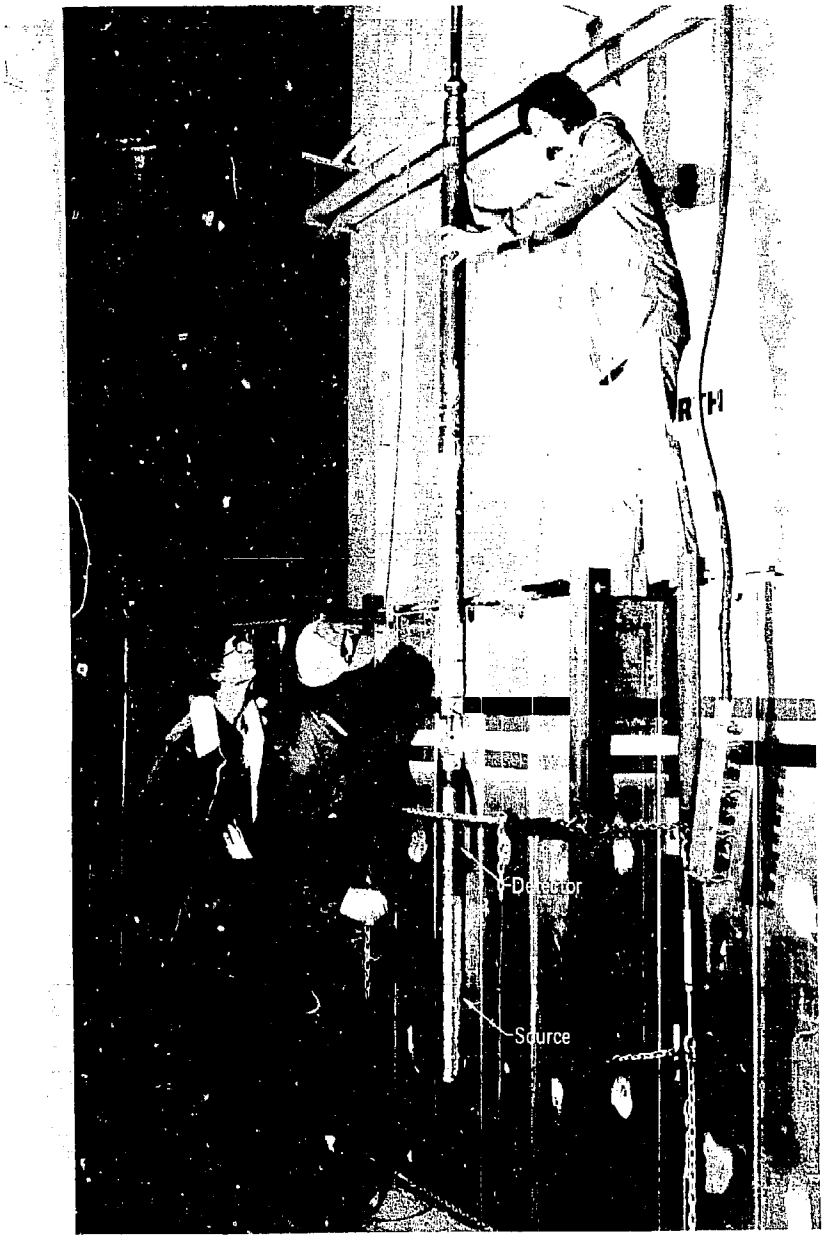

FIG. 3. Detail of a set of cells with a sonde (unshielded) in place on a flat face.

Sets of cells were used rather than tanks with boreholes for two reasons. First, it would be very difficult to fill a large volume with a controlled, partially saturated mixture because a vibrator large enough to vibrate many tonnes was unavailable to pack the fill material. Second, the amount of material required to surround a 2- or 3-m borehole with a thick layer of material of carefully controlled water content and density would be prohibitively expensive.

The cells contain sand, active alumina, tabular alumina, glass marbles, and water. The filling method and detailed discussion of the contents of each cell is discussed in Hearst (1979). The correction for the nominal density and water content of each cell to account for the 3-mm thick aluminum cell walls is indicated in Table 1. Because the cells sometimes bulge, there are gaps of up to 5 mm between some parts of some of the cells.

Figure 4 is a cross plot of density and water content (I_H) of the 12 sets of cells. The particular values of density and water content were chosen

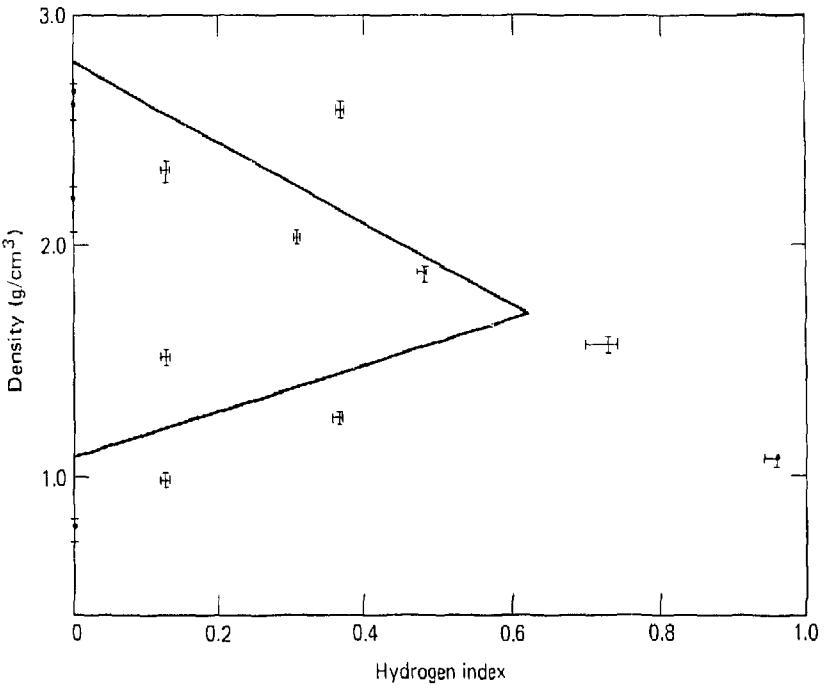

FIG. 4. Values of density and water content in the 12 cells. The triangle shows plausible field values.

Table 1. Contents of the 12 sets of cells in the HCTF.

Point	Component 1	Component 2	Free Water	Water content (Vol frac.)[a] Mean	Mean	Error for 0.3-cm gap	Bulk density, g/cm[a] Mean	Mean	Error for 0.3-cm gap
1	Dry active alumina	--	no	0.	0.		0.815 ± 0.011	0.89	0.02
2	Tabular alumina	--	no	0.	0.		2.09 ± 0.03	2.10	0.04
3	Tabular alumina	sand	no	0.	0.		2.64 ± 0.02	2.63	0.05
4	Partly saturated active alumina	--	no	0.130 ± 0.003	0.125	0.002	0.92 ± 0.01	0.99	0.02
5	Partly saturated active alumina	sand	no	0.132 ± 0.004	0.126	0.002	1.48 ± 0.01	1.51	0.03
6	Glass marbles	sand	yes	0.133 ± 0.002	0.127	0.002	2.3 ± 0.01	2.32	0.05
7	Saturated active alumina	--	no	0.38 ± 0.003	0.364	0.007	1.2 ± 0.002	1.26	0.02
8	Sand	--	yes	0.321 ± 0.001	0.308	0.006	2.02 ± 0.01	2.03	0.04
9	Tabular alumina	--	yes	0.383 ± 0.002	0.367	0.007	2.58 ± 0.004	2.58	0.05
10	Active alumina	sand	yes	0.500 ± 0.002	0.48	0.01	1.86 ± 0.01	1.89	0.04
11	Active alumina	--	yes	0.755 ± 0.016	0.73	0.015	1.54 ± 0.01	1.58	0.03
12	None	--	yes	1.000	0.96	0.02	1.000	1.07	0.02

[a]Corrected for aluminum.

to span the region of plausible field values of porosity less than 60% and grain density between 2.8 and 2.65 g/cc. The error bars arise primarily from uncertainty (taken as 3 mm) in the size of the gaps between the cells.

INTERPOLATION ALGORITHMS

Our objective is to obtain a method of estimating the hydrogen index I_H from the density (ρ), count rate (N_N), and gap between the sonde and borehole wall (G). In this section we discuss ways in which such an algorithm could be developed and how the systematic and fluctuating errors from the algorithm could be evaluated.

We presume there exists an exact functional relationship by which I_H could be calculated from ρ, G, and the average count rate N_N that would be measured if the sonde were to sense a homogeneous medium for a long time:

$$I_H = F(\rho, \bar{N}_N, G) \quad . \tag{1}$$

For a given measurement with the sonde, we have observed values indicated by the subscript k

$$\rho_k = \rho + e_\rho \quad ,$$

$$N_{Nk} = \bar{N}_N + e_N \quad ,$$

$$G_k = G + e_G \quad ,$$

where we assume that the errors e are zero-mean independent random variables with standard deviations σ_ρ, σ_N, and σ_G. When the log is run in a hole, I_H is estimated from measurements by use of a postulated functional relationship that we write as H; i.e.,

$$\hat{I}_H = H(\rho_k, N_{Nk}, G_k) \tag{2}$$

where the symbol "^" indicates the estimate of a parameter. The uncertainty in any measurement of I_H is a random variable given by

$$\Delta I = \hat{I}_H - I_H \quad .$$

If there are systematic errors in the estimate, resulting, for example, from an incorrect choice of function, ΔI will not be zero-mean.

Assuming that the observation errors are small enough, we can write a first-order approximation for the error in the estimate:

$$\Delta I = \hat{I}_H - I_H = H(\rho,\bar{N}_N,G) - F(\rho,\bar{N}_N,G) + \delta I(\text{data}) \ , \tag{3}$$

where

$$\delta I(\text{data}) = \left(\frac{\partial H}{\partial \rho}\right) e_\rho + \left(\frac{\partial H}{\partial N_N}\right) e_N + \left(\frac{\partial H}{\partial G}\right) e_G \ ,$$

With our assumptions, the mean of δI (data) is zero, and the variance is given by

$$\sigma^2(\text{data}) = \left(\frac{\partial H}{\partial \rho}\right)^2 \sigma_\rho^2 + \left(\frac{\partial H}{\partial N_N}\right)^2 \sigma^2{}_{N_N} + \left(\frac{\partial H}{\partial G}\right)^2 \sigma_G{}^2 \ . \tag{4}$$

This can be calculated no matter how H is determined. Most published log calibrations use only a form of $\partial H/\partial N_N \, eN$ to estimate the uncertainty in I_H, a procedure that indicates the repeatability of the measurements but ignores the systematic error, (H-F).

Both the nature of the systematic error and our ability to estimate it depend on the method used to obtain the algorithm. If the function F could be derived correctly (and used without a calibration), then the only source of error would be δI(data), which is easily evaluated. However, because we do not know F, we must calibrate. The count rate response is measured for a number (m) of sets of I_H, ρ, and G. Postponing discussion of the error in our knowledge of the values of these variables in the calibrator, we assume that our measured count rates $N_N(i)$ differ from the correct count rates $N_N^O(i)$ by an additive random variable:

$$N_N(i) = N_N^O(i) + e(i) \text{ for } i = 1,m \ ,$$

where the calibrator properties are related to $N_N^O(i)$ by

$$I_H(i) = F\left[\rho(i),N_N^O(i),G(i)\right] \ . \tag{5}$$

The e(i) are assumed to be zero-mean, independent random variables with standard deviation $\sigma(i)$.

To indicate that the calibration algorithm is based on these measured count rates, we write

$$\hat{I}_H = H(\rho_k, N_{Nk}, G_k / \underline{N}_N) \ ,$$

where the symbols in front of the slash indicate the measurements in the borehole and the symbol after the slash represents the vector of calibration measurements $[N_N(i)]$. Again, assuming small errors and separating the systematic error into two terms,

$$\Delta I = \hat{I}_H - I_H = \delta I(\text{cal}) + \delta I(\text{fit}) + \delta I(\text{data}) \ . \tag{6}$$

The first term,

$$\delta I(\text{cal}) = \sum_{i=1}^{m} \left[\frac{\partial H}{\partial N_N(i)} e(i) \right] , \tag{7}$$

is a zero-mean, random variable whose variance is calculated from the differences in repeats of the calibration measurements,

$$\sigma^2(\text{cal}) = \sum_{i=1}^{m} \left[\frac{\partial H}{\partial N_N(i)} \right]^2 \sigma^2(i) \ . \tag{8}$$

The second term,

$$\delta I(\text{fit}) = H(\rho, \bar{N}_N, G / \underline{N}_N^O) - F(\rho, \bar{N}_N, G) \ , \tag{9}$$

is a fixed bias resulting from the choice of the algorithm. Whenever parameters based on a particular set of calibration measurements are used, the $\delta I(\text{cal})$ is a fixed bias. The equation for $\sigma^2(\text{cal})$ is used only to estimate how large that fixed bias could be.

The nature of these errors depends on how the form of the algorithm is chosen. Three curve-fitting methods are discussed here: (1) Using least-square methods to estimate parameters of a function known to have the correct form; (2) Using least-square methods to estimate parameters of arbitrarily chosen functions, and (3) drawing a curve by "eye".

If the functional form is known to be correct, then $\delta I(\text{fit}) = 0$. However, a systematic error persists because of uncertainties in the measurement of the calibration data points. Its properties can be derived from the least-squares theory. The uncertainty $\delta I(\text{cal})$ for a given set of parameters is unknown and varies with the independent variables (ρ, I_H, G). It is usually smallest close to the calibration points. The variance of $\delta I(\text{cal})$,

σ^2(cal), can be calculated. It decreases inversely with the number of degrees of freedom, or with the excess of independent calibration points over the number of parameters. Consequently, including enough parameters to describe the physics completely--and thereby making $\delta I(fit) = 0$--might make σ^2(cal) unacceptably large.

If the form of the algorithm is chosen arbitrarily, $\delta I(cal)$ behaves as described in the previous paragraph. In addition, there is an unknown bias, $\delta I(fit)$ from the inability of the function in the algorithm (H) to represent the real physics in F. Goodness-of-fit tests, which compare the residuals at the calibration points to $\delta I(cal)$, can determine if there is a poor fit. It is possible, in principle, to estimate the sum of the squares of the bias at the calibration points from such a test but very difficult to estimate it for regions between calibration points.

It is very difficult to assess $\delta I(fit)$ and $\delta I(cal)$ resulting when calibration curves are drawn "by eye". Consequently, one rarely sees discussions of the possibility of systematic errors when this type of fit is made.

OUR ALGORITHM

We developed an algorithm for I_H as a function of N_N, θ, and G by using method (2). Exact forms have been developed for N_N as a function of medium properties such as transport and scattering mean free paths, logarithmic energy decrement per collision, or diffusion coefficient (Tittle, 1961; Kozhevnikov, 1963). But we have found no solution that predicts I_H in terms of density and water content alone. We developed and investigated several such forms with some basis in neutron physics, restricting ourselves to five parameters to minimize calibration uncertainty.

The forms we studied represented the count rate as the dependent variable so that the goodness-of-fit was evaluated by comparing the residuals of the count rate to the measurement uncertainty. Although all forms we used failed this test, we eventually chose one giving the smallest sum of residuals. This was done for a few cases (e.g., large hole, dry; small hole, wet), and then the same form was applied to all the cases. Recognizing that the form does not adequately describe the physics, we must estimate $\delta I(fit)$ by other means. Our justification for using this form is given in the Appendix.

The function finally chosen for zero-gap data was

$$y = \ln N_N = a_1 (1 + a_2\rho) \exp(a_3 I_H) + a_4 . \qquad (10)$$

A plausible correction term for gap G was then included:

$$y = \ln N_N = a_1(1 + a_2\rho)\exp(a_3 I_H) + a_4 \quad \times \begin{cases} 1+a_5 G\, I_H & \text{for dry holes} \\ 1+a_5 G(1-I_H) & \text{for wet holes} \end{cases} \qquad (11)$$

Point No. 1 ($I_H = 0$, $\rho = 0.89$) was not used in the fitting procedure because its count rate is less than that for point No. 2. This decrease is caused by a reduction in scattering at very low density and water content, and while it makes physical sense (Hearst, 1979), it would require extra parameters to fit. We were, therefore, left with 11 calibration points.

The computer code "ZXSSQ8" (IMSL, 1978) was used to determine the non-linear least-squares fit of the data in the following manner. First, the logarithm of the measured counts (in API units) was taken, and the coefficients (a_1, a_2, a_3, a_4) were determined by fitting Eq. 10 to the zero-gap data alone. Second, the fifth coefficient was determined alone by using the previously determined (a_1, a_2, a_3, a_4) coefficients, fitting Eq. 11 to all of the data. These a_i coefficients are given in Table 2 for two sizes of sondes in dry and wet holes, both large and small. A sample set of API counts is given in Table 3.

The relationship above must be solved for water content by a root-finder or iterative technique since it cannot be inverted for non-zero value of gap. Plots of typical algorithms of count rate vs water content for various values of density and gap are given in Figs. 5 (a-e).

The algorithms in Fig. 5 have a shape consistent with those from service companies (Tittman, et al., 1966). Their curves are always plotted at 100% saturation. For comparison, curves equivalent to 100% saturation in a material of matrix density of 2.65 are shown as dashed lines in Figs. 5 (a-e).

ERROR ANALYSIS

There are four sources of error (or uncertainty) in the water content calculated by applying the algorithm to the output of a neutron log.

Table 2. Coefficients of the algorithm for one small sonde and the big-hole sonde, including estimated error in the measured count.

Sonde size	Hole size	Wet or dry	Shield	a_1	a_2	a_3	a_4	a_5	σ_y^2 exp
small	big	dry	no	2.9562	-0.0965	-2.7438	5.5562	0.1613	3.47×10^{-4}
small	big	dry	yes	3.2525	-0.0758	-2.5015	5.4379	0.2750	2.2×10^{-5}
small	big	wet	no	3.9320	-0.11116	-3.2335	5.3275	-0.0529	7.6×10^{-4}
small	big	wet	yes	3.4581	-0.09958	-3.3510	5.5749	-0.0533	1.33×10^{-3}
small	small	dry	no	1.3302	0.2720	-2.8675	7.3279	0.0605	1.57×10^{-3}
small	small	dry	yes	2.580	0.0369	-2.6198	6.1982	0.1806	3.49×10^{-3}
small	small	wet	no	3.904	-0.883	-3.311	5.3437	-0.0854	7.81×10^{-4}
small	small	wet	yes	3.6237	-0.0739	-3.2370	5.6005	-0.1751	3.54×10^{-4}
big	big	dry	built-in	3.919	-0.0923	-2.7666	4.8326	0.3727	5.0×10^{-4}
big	big	wet	built-in	4.2502	-0.1026	-3.1696	4.9108	-0.1448	3.6×10^{-4}

Note: Small sonde is No. 193. Coefficients for the other small sondes are similar.

Table 3. Set of calibration data for one small sonde and the big-hole sonde.

Sonde size	Hole size	Wet or dry	Shield	Counts per second for point No. 1	2	3	4	5	6	7	8	9	10	11	12
small	big	dry	yes	253	251	252	161	141	132	61	67	44	39	27	24
small	big	wet	yes	279	361	327	143	131	125	56	63	42	35	25	24
small	small	dry	yes	409	665	661	269	261	248	110	142	109	89	60	47
small	small	wet	yes	355	512	389	194	185	168	65	72	51	44	31	26
small	small	wet	no	311	420	345	165	147	113	54	73	39	35	22	18
big	big	dry	built-in	272	310	257	158	131	116	52	57	33	28	20	17
big	big	wet	built-in	347	447	302	179	141	121	52	55	35	29	20	17

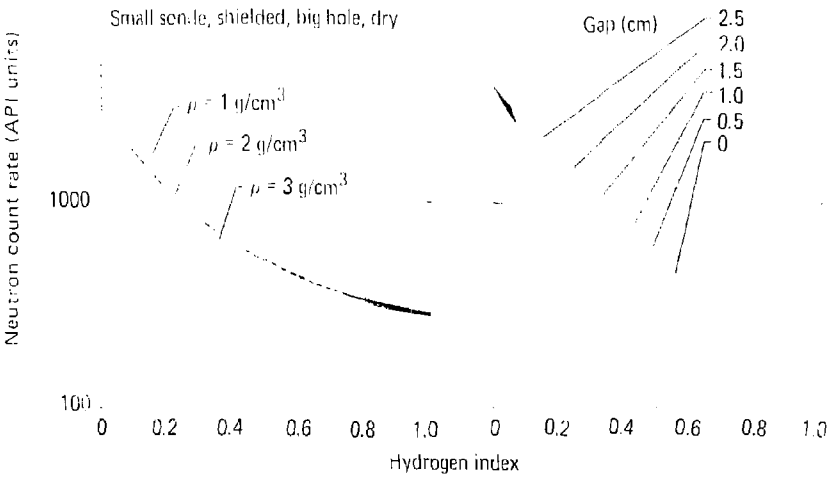

FIG. 5a. Algorithm for I_H as functions of count rate for different densities at zero gap (left curves) and different gaps at density 2 g/cc (right curves). Small sonde, shielded, big hole, dry.

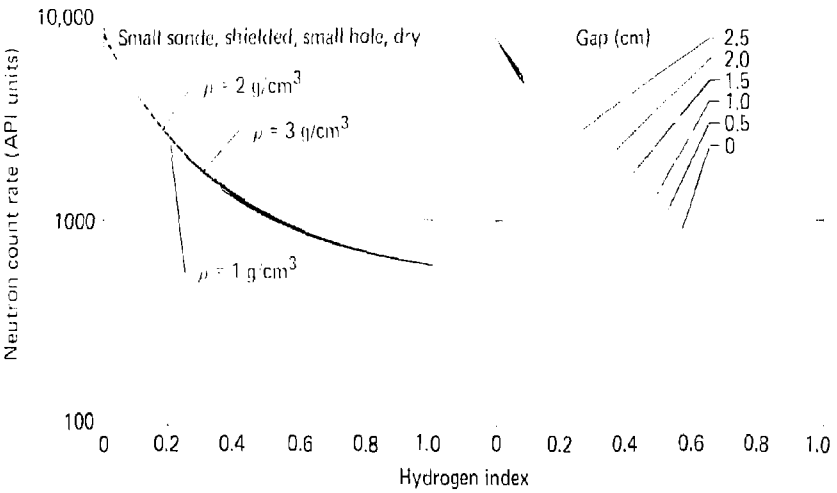

FIG. 5b. Algorithm for I_H as functions of count rate for different densities at zero gap (left curves) and different gaps at density 2 g/cc (right curves). Small sonde, shielded, small hole, dry.

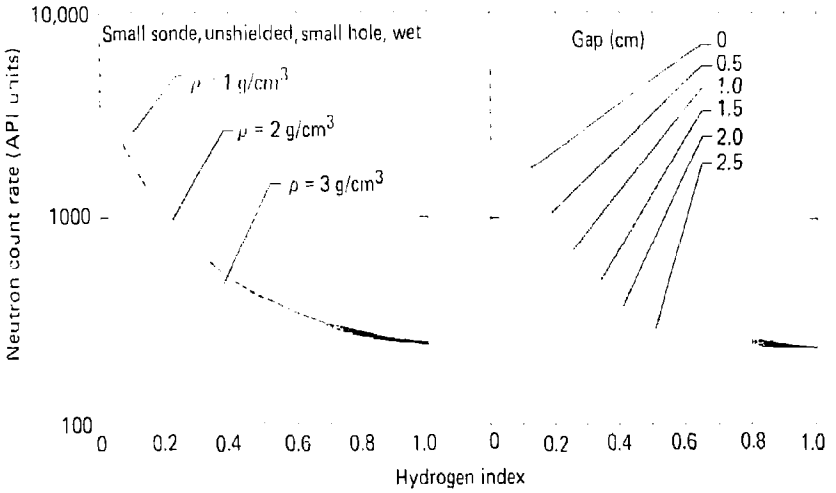

FIG. 5c. Algorithm for I_H as functions of count rate for different densities at zero gap (left curves) and different gaps at density 2 g/cc (right curves). Small sonde, no shield, small hole, wet.

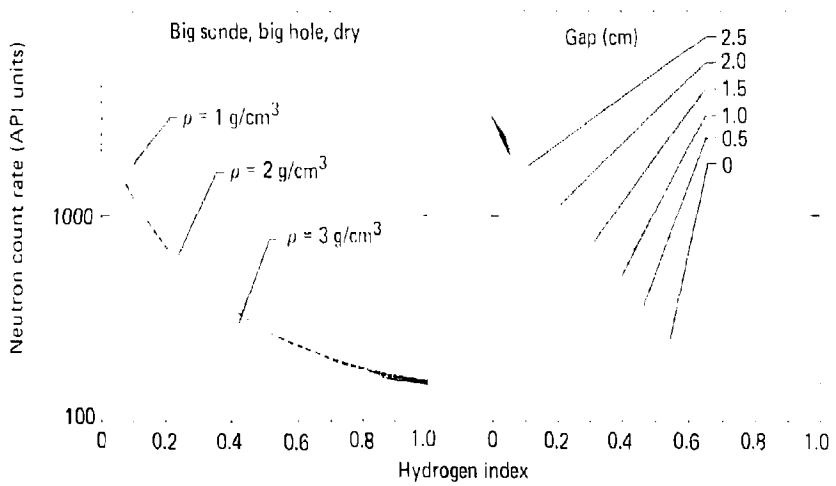

FIG. 5d. Algorithm for I_H as functions of count rate for different densities at zero gap (left curves) and different gaps at density 2 g/cc (right curves). Big-hole sonde, dry.

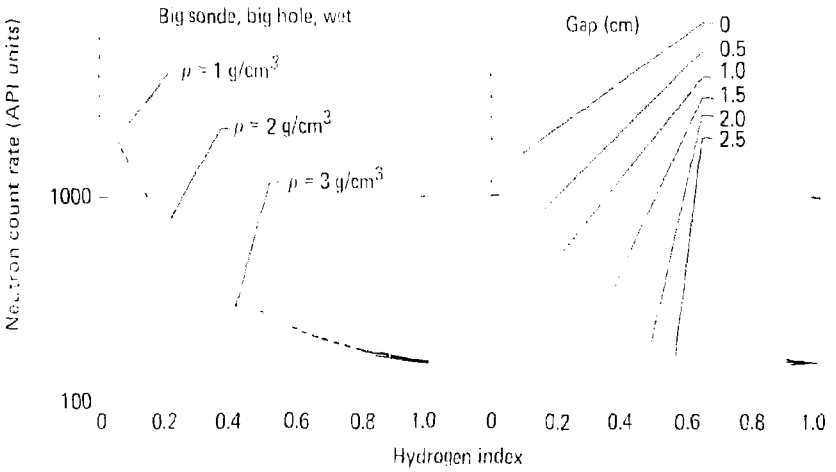

FIG. 5a. Algorithm for I_H as functions of count rate for different densities at zero gap (left curves) and different gaps at density 2 g/cc (right curves). Big-hole sonde, wet. Dashed line is density for 100% saturation with matrix density of 2.65.

(1) Imperfections in the measurements: these arise from statistical uncertainties in the count rate and from other uncertainties in the output of the sondes.

(2) Imperfections in the algorithm: these arise because the algorithm is not a good description of the phenomena of neutron logging.

(3) Imperfections in the test facility: these arise because the HCTF is not really a borehole but rather a set of aluminum cells in a building.

(4) Imperfections in the world: these arise because the calibration assumes that the borehole is surrounded by an infinite, isotropic, homogeneous medium, and it is not.

The sources of uncertainty are outlined in Table 4.

IMPERFECTIONS IN THE MEASUREMENTS

Error caused by imperfections in the measurements, both in the field [δI(data)] and in the calibration facility [δI(cal)], can be evaluated.

Table 4. Summary of the sources of uncertainty at the HCTF.

Source of Uncertainty	Eq. No.	Fluctuating or systematic	Comments
IMPERFECTIONS IN THE MEASUREMENTS			
Sonde-wall gap	4	F	Use sonde with two gap indicators.
Bulk density	4	F	Has small effect.
Counting statistics	15	F	Average over long times (20 s).
Count uncertainty in calibrator	15	S	Cannot eliminate, but small.
IMPERFECTIONS IN THE ALGORITHM			
Bias in algorithm	9	S	Cannot eliminate, not necessarily small.
IMPERFECTIONS IN THE FACILITY			
Nonuniformity of cells		S	Is apparently negligible.
Variation with height		S	May be important.
Floor of calibrator		S	Cannot eliminate. Quite small for large holes, possibly exists for small holes.
Gaps between cells		S	Cannot eliminate, probably small.
Gap between water-filled cell and others		S	Redesign small, wet calibration if needed.
Squareness of small hole		S	Redesign small, wet calibration if needed.
Flat face of big "hole"		S	Add shielding to sonde, or apply a correction.
Alumina instead of silica		S	Cannot eliminate, but probably unimportant.
IMPERFECTIONS IN THE WORLD			
Nonuniformity of medium surrounding borehole	19,20	F	Recognize nonuniformity and calculate a correction.

Since the final algorithm for I_H is not written analytically, the partial derivatives in Eqs. 4 and 8 must be evaluated indirectly from

$$y = y(\rho, I_H, G/N_N) \quad , \tag{12}$$

where y represents the natural logarithm of N_N. For example,

$$\frac{\partial I_H}{\partial \rho} = \frac{\partial I_H}{\partial y}\left(\frac{\partial y}{\partial \rho}\right) = \frac{1}{\partial y / \partial I_H}\left(\frac{\partial y}{\partial \rho}\right) \quad . \tag{13}$$

Three uncertainties contribute to the variances of $\sigma I(\text{data})$ and $\sigma I(\text{cal})$: sonde-wall gap, density, and count.

UNCERTAINTY IN THE SONDE-WALL GAP

An uncertainty in the gap gives rise to the σ_G^2 term in Eq. 4. The small-hole sonde, which has a proximity indicator only at its upper end, can have large uncertainties if it is not parallel to the wall. We have studied a similar sonde (a density sonde) with two indicators and found that for a rough hole the difference between the gap seen by the upper indicator and the average gap can have a mean σ_G as large as 0.3 cm. This in turn can lead to uncertainties of as much as 10% in I_H (at $I_H = 0.5$), certainly unacceptably large from a single source of error. We will reduce this problem by using a big-hole sonde with two gap indicators, which should reduce the uncertainty to less than 0.1 cm.

UNCERTAINTY IN THE DENSITY

We require bulk density, and, therefore, the output of a density log, to obtain I_H from Eq. 10. We have found that the density logs we use can be in error by as much as 5% under normal circumstances. However, when this value, (or $\sigma_\rho = 0.05\ \rho$) is used in Eq. 4, it makes only a small contribution to $\sigma^2(\text{data})$.

UNCERTAINTY IN THE COUNT

The count N_N is Poisson-distributed, so one would expect that $\sigma^2_{N_N} = N_N$. However, N_N is recorded in API units, obtained by multiplying the true count rate N'_N by a constant that we shall call M. Therefore,

$N_N = MN'_N$, and that part of $\sigma^2_{N_N}$ attributed to counting statistics is MN_N. In addition, there is some experimental error caused by nonrepeatability of placement of the sonde against the borehole wall. We have chosen to include this term in $\sigma^2_{N_N}$. We have estimated it from data taken in the calibrator by finding the mean square residual of the count for repeated setups at each calibration point. If the logarithm of this residual is plotted as a function of I_H and ρ, no systematic variation is found. Therefore, we assume that the residual $\sigma^2_Y(\text{exp})$ is a constant, and thus,

$$\sigma^2_{N_N}(\text{exp}) = N^2_N \sigma^2_Y(\text{exp}) \quad . \tag{14}$$

Note that $\sigma^2_Y(\text{exp})$ is given in Table 2. Combining these two terms, then

$$\sigma^2_{N_N} = MN_N + N^2_N \sigma^2_Y(\text{exp}) \quad . \tag{15}$$

If the count is averaged over one time constant of the system, the variance is inversely proportional to that time constant. The time constant for our logs is 2 or 3 s. (It is 100 s in the calibrator, effectively eliminating that source of uncertainty.) If a value of M appropriate to 2 s is used in Eq. 15, with $\sigma_{I_H} = \sigma_G = 0$, uncertainties of 10 to 15% are seen in the I_H (at values of 0.1 to 0.6) for the big-hole dry case and 8 to 12% (for values up to 0.4) for the small-hole unshielded case--the standard oil field situation. Since the slope of the algorithms is most shallow at large I_H, the uncertainty is greatest at large I_H. Evidently the count rate in some other service-company systems is much greater than in this one, greatly reducing this source of uncertainty (Tittman, et al., 1966).

If, however, we average over 20 s, the effect is reduced to about 4% of the value. Normal logging speed is about 9 m/min for this type of log, so taking a running average over 3 m is a plausible solution to the time constant problem. (We have chosen 3 m as our normal averaging distance for this and other logs.)

The properties of the sonde's detector and electronics can change with time. Field calibration must be used and noted to be sure that these changes are dealt with in data reduction. Our procedure is to monitor the constant M required to convert from count rate to API units.

An illustration of the uncertainties can be seen by plotting various estimates of δI as functions of I_H. Figure 6 shows two sets of data for each case. The solid line is the calculated value of σ(cal), the bias caused by measurement errors in the calibrator. The dashed line shows $\sqrt{\sigma^2(\text{cal}) + \sigma^2(\text{data})}$ for a realistic field case, with $\sigma_\rho = 0.04$, $\sigma_G = 0.12$ cm, and a time constant of 20 s. We will use these dashed lines as an estimate of uncertainty caused by imperfections in the measurements.

IMPERFECTIONS IN THE ALGORITHM

After we fit our algorithm to the data in the various cases, we made an F-test in "y" space to compare the residuals $\hat{I}_H - I_H$ to the differences among repeat measurements. In all cases, lack of fit was shown, and therefore, δI(fit) is not zero.

One source of bias can be seen in Eq. 11, where the bulk density appears only as a coefficient of $\exp(a_3 I_H)$, and a_3 is negative. Consequently, at large I_H the density effect becomes very small. Therefore, Eq. 11 is unable to reproduce all of the effect of density on N_N that is seen in the calibrator at $I_H = 0.36$.

Another source of bias arises because point No. 1 was not included in the fit, and the N_N was not required to go to zero at $I_H = \rho = 0$.

The bias that results from using inappropriate fitting functions is difficult to evaluate. We used two approaches to determine bias: one estimated it near the calibration points and the other estimated it elsewhere. The bias at the calibration points is estimated from the sum of the residuals at a calibration point

$$\frac{1}{j} \sum_j (\hat{I}_H - I_H) \approx \sum_j \left[\delta I(\text{fit}) + \delta I(\text{cal}) + \delta I(\text{data})\right] , \qquad (16)$$

where the sum is taken at a single calibration point over all j cases (e.g., big hole, dry; small hole, wet), and δI(data) is the measurement error in the calibrator.

Since the measurement errors for the different cases are reasonably assumed to be independent, the last two terms do not add constructively. The

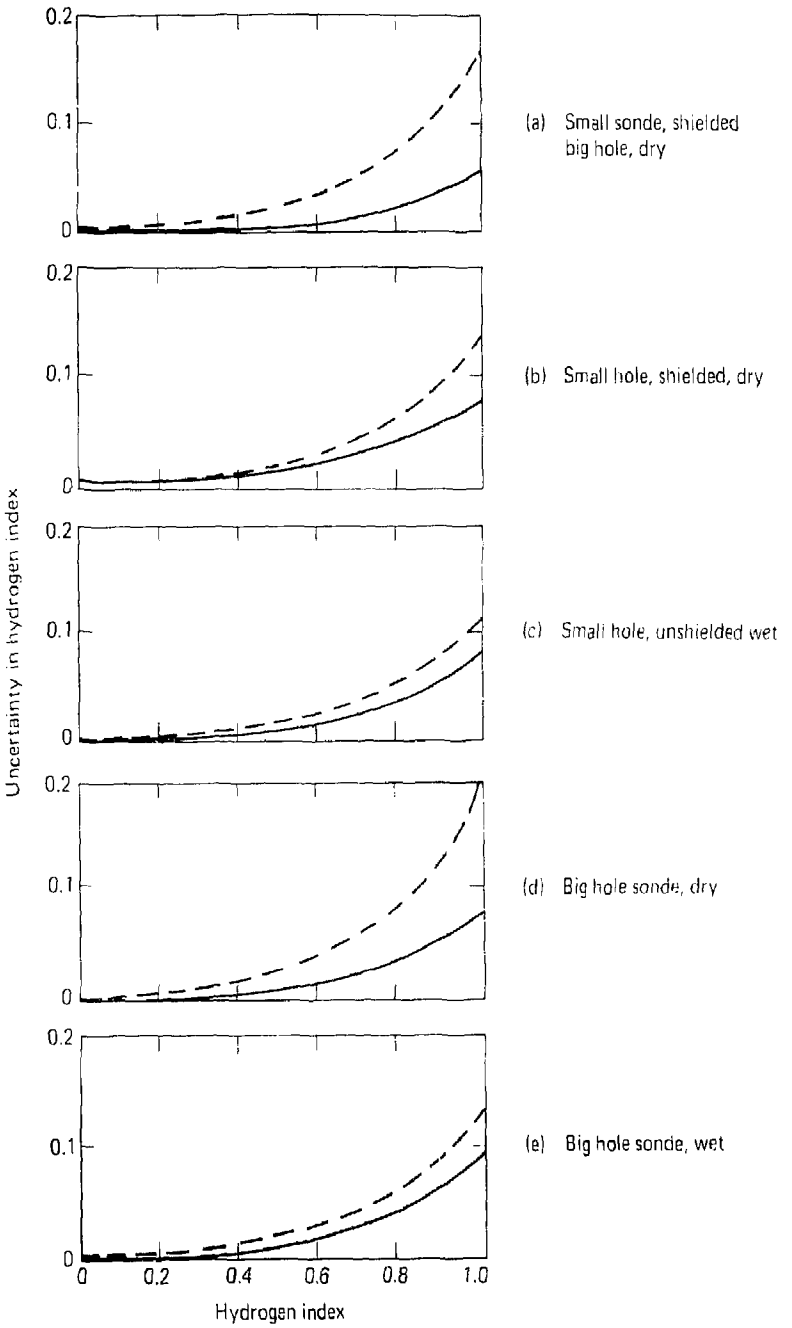

FIG. 6. Uncertainty in the water content calculated from the algorithms. Density is 2 g/cc, gap 2.5 mm. Solid line is σ(cal) only. Dashed line includes density uncertainty of 4%, gap uncertainty of 1.2 mm, and a 20 s time constant.

average residual is then approximately the average bias for the ρ-I_H point represented by that calibration point. Figure 7 shows the average residual for 10 zero-gap cases. In the plausible region (the triangle) the magnitude of the bias is never more than 0.02; the shape of the bias function seems similar for all cases. The algorithm tends to overestimate I_H for I_H up to about 0.2 and underestimate it between about 0.2 and and 0.5.

Another way to estimate the bias between calibration points is to fit the calibration data by a completely different method. The potential misfit bias

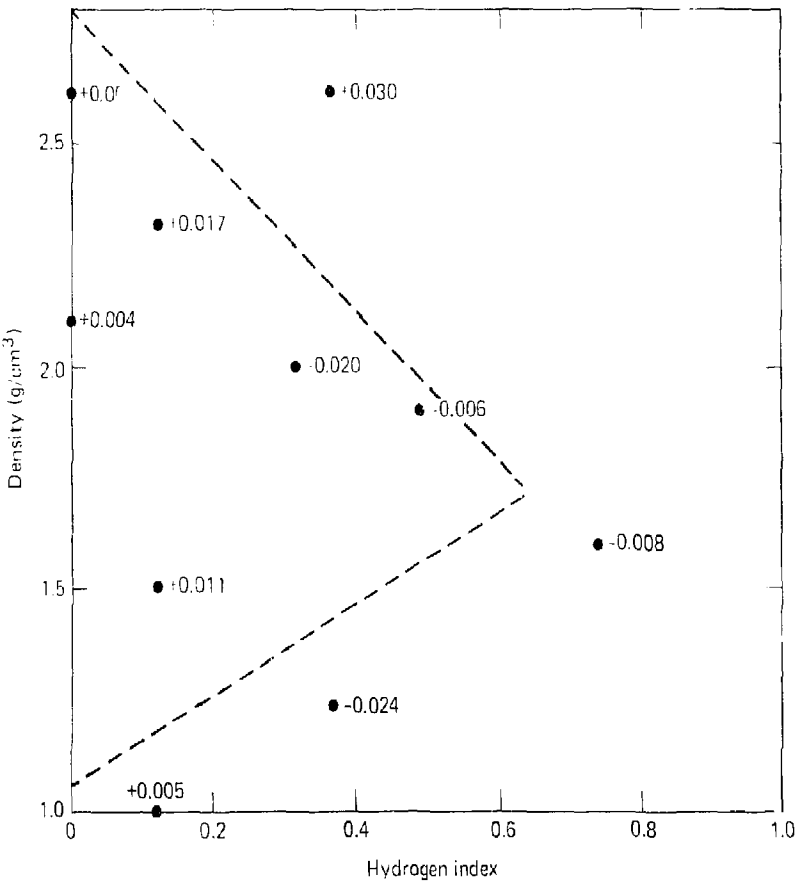

FIG. 7. Mean values of residual between calculated and true I_H, where the mean is taken over all measurement cases at each calibration point. This can be interpreted as the bias.

is at least as large as the difference between two equally plausible fitting methods. Figures 8 (a-b) demonstrate the difference between our algorithm and a surface drawn through the zero-gap calibration points by a geostatistical method called "Kriging" for two different cases (see, for example, Delhomme, 1978). Kriging is an interpolation method that determines the best linearized unbiased estimator of a surface [in this case $I_H = U(\rho, N_N)$] that has been sampled at a finite number of irregularly spaced points. Since we have no a priori reason to assume that the Kriged surface is a better or worse estimate than our algorithm, we use the difference between them as a

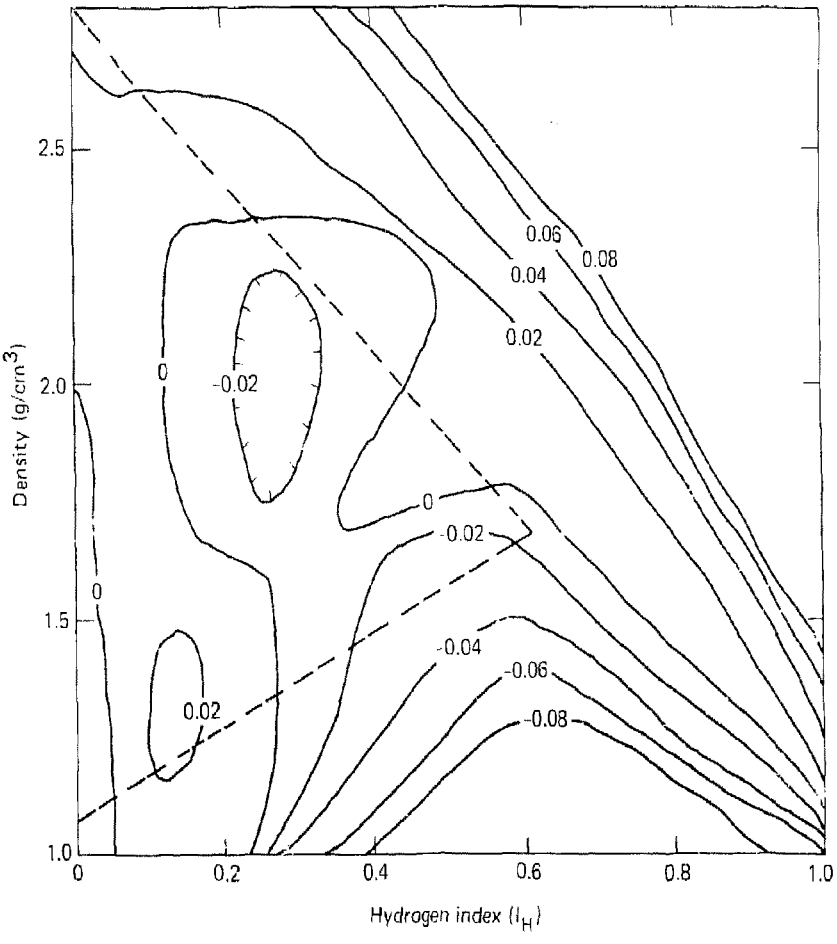

FIG. 8a. Contours of difference between I_H calculated from our algorithm and from the geostatistical method known as Kriging. Big sonde, big hole, dry.

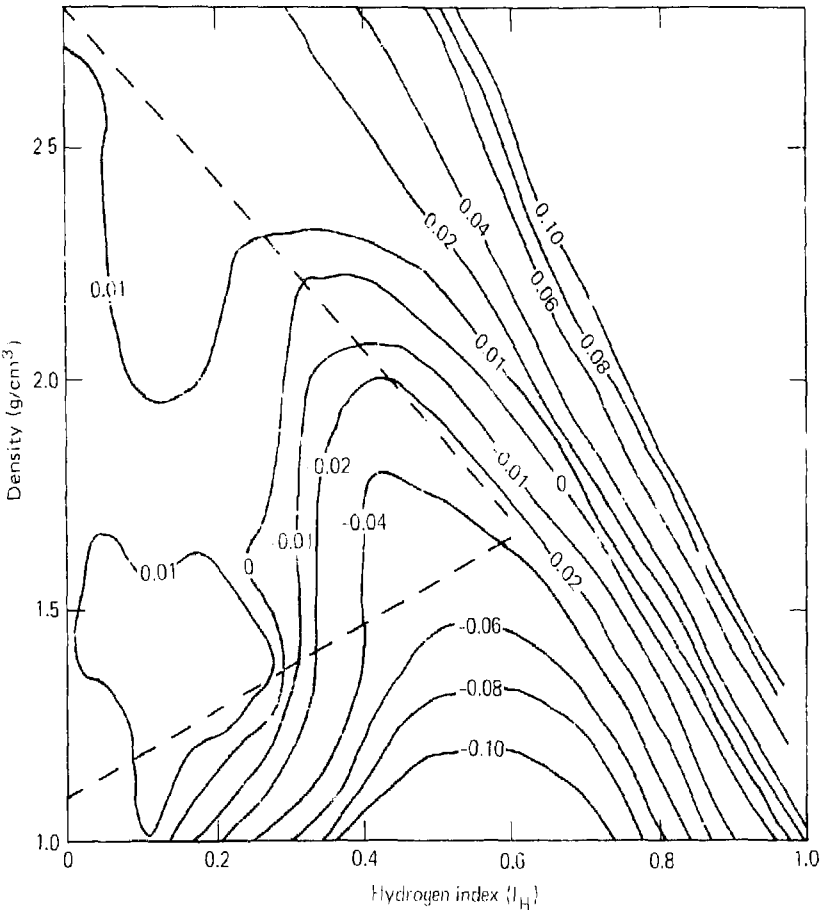

FIG. 8b. Contours of difference between I_H calculated from our algorithm and from the geostatistical method known as Kriging. Small sonde, small hole, wet.

measure of how large the bias could be using either of them. As can be seen in Fig. 8, the absolute difference in the plausible region rarely exceeds 0.025, and usually is less than 0.02. This raises our confidence in the use of our algorithm.

IMPERFECTIONS IN THE TEST FACILITY

NONUNIFORMITY

Considerable effort was expended to assure the uniformity of the contents of each measurement cell. Nonetheless, perfect uniformity cannot be guaranteed. Furthermore, the cells bulge, and consequently the sonde is not in perfect contact with the cell over its entire length. Finally, there can be a few degrees of rotation of the sonde about its axis between readings on the cells. These phenomena give rise to variations of no more than 2% at a given place and were used to calculate $\sigma^2(i)$.

The normal calibration measurements for the big-hole case were made with the sonde centered on the cell. Some measurements were made with the sonde 30 cm higher. When this was done, in some cases the count rate changed enough to alter the calculated f_{II} by as much as 0.02. However, the direction of the change varied apparently randomly, and the mean over all of the cell sets was less than 0.0025. One can imagine many possible causes for such changes, but we have not been able to identify any specific causes. We did not include these variations in data points in the big-hole calibration and therefore did not include the variation in $\sigma^2(i)$.

As a test of the importance of the variability with position, we fit Eq. 9 to the count rates representing the most different numbers of counts at the high and normal positions for each set of cells. When this was done, the result satisfied an F-test in "y" space. In addition, the result implies that the scatter in the data is enough to account for all of the scatter about the fitted curve and that while $\sigma(\text{fit})$ may be eliminated, $\sigma(\text{cal})$ has become much larger.

A calculation of $\sigma(\text{cal})$ like that shown in Fig. 6 indicates that this is indeed the case. When these extreme data are used to calculate the total uncertainty, only $\sigma(\text{cal})$ and $\sigma(\text{data})$ are needed. A curve like the dashed line in Fig. 6 shows this total uncertainty, which becomes as much as 11% of I_{II} when both the high and normal data are included in the fit.

FLOOR OF THE BUILDING

One possible cause of the variation with height is the floor of the building. The cells in the test facility are 2-m high and rest on a concrete floor. One would expect that neutrons reflected from the floor would have an effect on the data and, indeed, they do. We tested the effect of the distance from the floor in the big-hole geometry by varying that distance with the front of the sonde touching a cell (the normal arrangement) and also with the back of the sonde touching a cell. The effect was large in the latter case. In the former, as discussed above, the mean effect was very small, and so the variation cannot be attributed to only height from the floor.

In the small-hole configuration, the mean of the effect of height over all data points was less than its overall standard deviation, but the mean was larger and the count rate always decreased when the sonde was raised. Therefore, the effect appears to be real with a maximum of perhaps as much as 0.025. Consequently, all the data used in the small hole were taken at the higher calibration point to minimize the floor effect. (We are, however, unable to prove the effect has been eliminated, since there is no way of raising the sonde farther and still obtaining a calibration.)

GAPS BETWEEN THE CELLS

A gap of 0.3 cm surrounding each cell would increase the cell area by a factor of 1.02 and thus decrease the apparent density and water content by a factor of 0.98. This would then decrease the water content in a set of cells by about 2% of its value--if there were a gap that large, totally surrounding all cells. However, the sonde is always pressed tightly against the face of a single cell whose density and water content are well-known, so the apparent density and water content are influenced primarily by those of the single cell. Moreover, the cells are always touching one another at one point (usually the center) so that while gaps of this size can, in fact, be seen between cells, they are by no means uniform. It is therefore probable that the effect of these gaps is less than a tenth of the maximum possible value or less than 0.2% of the water content.

A gap between a cell full of water that is used to simulate a water-filled hole and the other cells in the array can give rise to another source of error. It will cause an increase in count rate and, therefore, a decrease in apparent water content. If we assume that the increase is the same as that caused by a similar gap between sonde and borehole in a dry, small-hole configuration, we find that the maximum count rate change is 250 API units for a 0.6-cm gap. The gap between a water-filled cell and others is not likely to be more than 0.3 cm (and usually much less), so we assume 125 API units.

This can give rise to substantial errors at high water content, but at values below a volume fraction of 0.35 the error is less than 10% of the value. This is again a maximum possible error and is not likely to occur in many cell sets. In fact, however, very large residuals were observed on one cell set (No. 8, water content 0.31) for all of the wet, small-hole cases. We attribute this to the gap. Because removing point No. 8 data from those calibrations greatly improved the fits, point No. 8 was not used in the wet, small-hole fits. In the big-hole case the water container was constructed to minimize this gap and eliminate it at the point of contact between the sonde and the cell it touches. No large residuals were observed. It is therefore reasonable to believe that except in the case of the small-hole set, the effect is negligible.

HOLE SHAPE

The small holes in the calibration facility are, of course, square. The logging service company that supplied the logging sonde has its own calibration facility with round holes. The company has published "limestone" calibrations of API units vs water content plus a chart for converting these to sandstone equivalents. Because sandstone is the closest to our silica-alumina mix, we chose a number of values of sandstone porosity, including those corresponding to the actual values surrounding the 30-cm holes in the company's test pits. We then used the conversion chart to change the sandstone values to their limestone equivalents. Next we looked up the number of API units on the company's limestone calibration curves for 30-cm holes, water-filled and dry, to compare those values to our "saturated" calibration curves. Our results are shown in Figs. 9 (a-b).

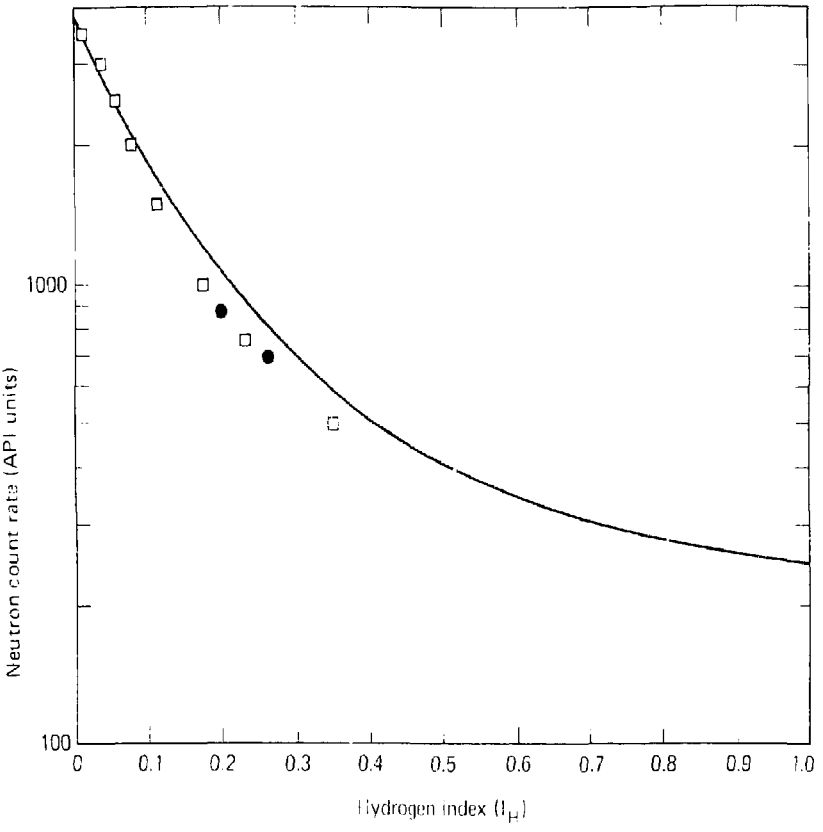

FIG. 9a. Comparison of logging company's calibration with our algorithm for a 20-cm diam hole, saturated sandstone (Squares represent the company's calibration curve, circles refer to points on that curve at values of I_H for which company had data). Water-filled hole.

We found that in the dry-hole case agreement was very good at the values of I_H equivalent to the company's data points, but our algorithm gives an I_H greater by 0.02 than the company's at low water content. In the wet-hole case, agreement is good at low water content, but our algorithm overestimates I_H at the data points by 0.04--evidently because we have water in parts of the hole where in a round hole there would be rock.

There are, of course, other reasons besides the shape of the hole for these differences. For example, we had to use a jack to urge the sonde against the face of the hole, and the company did not. Furthermore, the company used only two data points from 30-cm holes; otherwise, its curves are

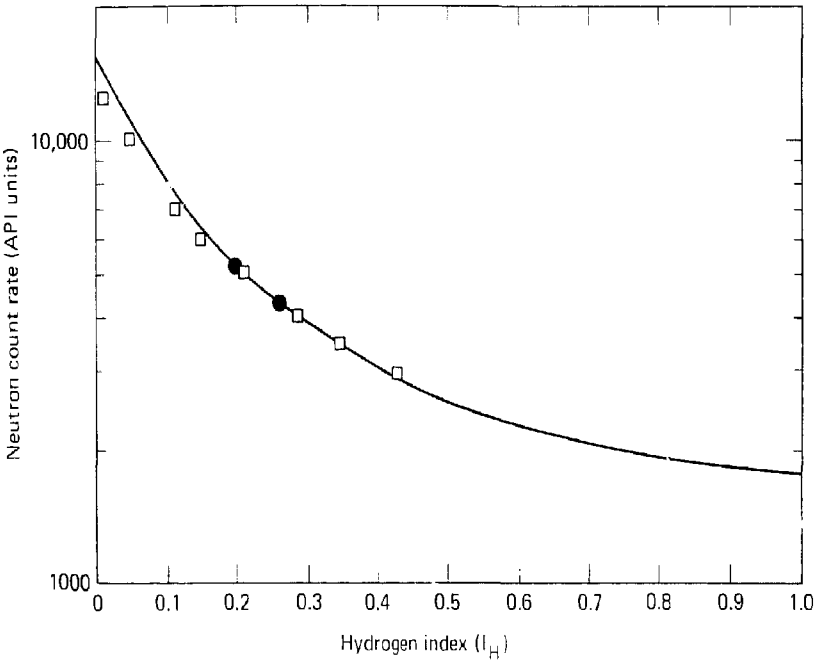

FIG. 9b. Comparison of logging company's calibration with our algorithm for a 30-cm diam hole, saturated sandstone (Squares represent the company's calibration curve, circles refer to points on that curve at values of I_H for which company had data). Dry hole.

extrapolated from data in smaller holes. Finally, the calibrations were made years apart with different sondes. Given these sources of differences, we can conclude that the square hole is not a major source of error for dry holes. However, if this calibration is to be used routinely in wet holes, there should be further study to see if a "hole-shape" correction should be applied in the wet-hole case.

The flat face of the calibration facility is intended to simulate a very large (2- to 3-m diam) hole. Two experiments were performed to test whether this simulation is satisfactory. In the first, a concrete block 3-m square and 0.5-m thick was placed in the aisle behind the sonde and moved various distances from it to test the effect of the back of a hole. With no shield on the sonde the change in apparent I_H varied from as much as 0.2 at 1 m to as much as 0.005 at 3 m. The change was a function of the water content of the cell on which the sonde was placed. With a shielded sonde the effect vanished for all distances more than 1.25 m--the smallest hole we expect to use.

In the second experiment, mock holes were built out of sandbags to test the effect of the sides of the hole. A coil with a face having a radius of curvature of 1.2 m was filled with a sand-water mix of known density and water content and placed in a trench so its face was level with the ground surface (Fig. 10). When the coil sonde was placed on this cell in a hole 2.5-m diam, the [illegible] decreased by 0.07 (out of 0.29) for the shielded sonde and by 0.11 without shielding. Our shield, then, is inadequate.

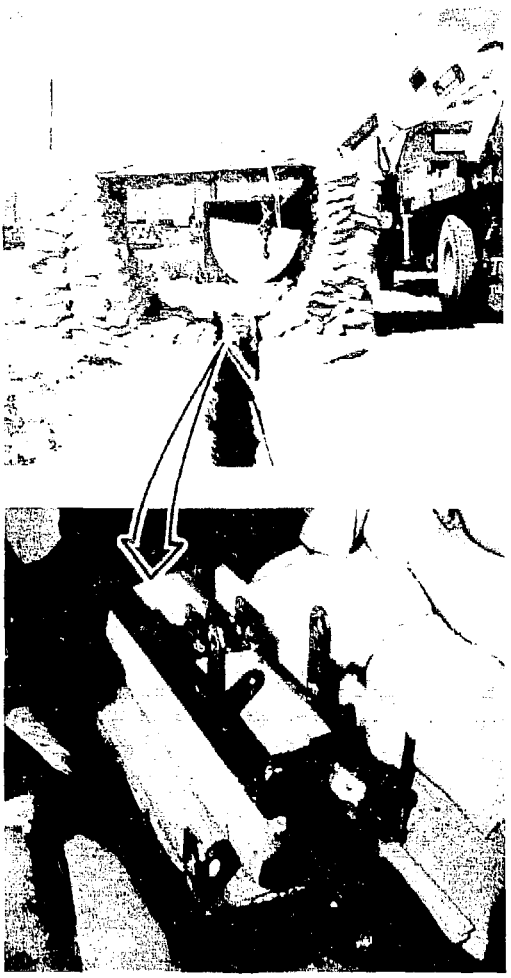

FIG. 10. Mock 2 m-diam hole for hole-size effects test. The working part of the big-hole sonde is shown on the test cell. One side has extra shielding.

The effect with the big-hole sonde was 0.03, presumably reduced by its thick shield. It is obviously necessary to apply a correction for this hole-size effect. Further experiments showed that if 7.5 cm of shielding were added to the sides of the big-hole sonde, the effect was eliminated for holes of 2-m diam or greater. As a result of this experiment we have decided to use only the big-hole sonde, with added shielding, in big holes.

MATERIALS

Most of the materials at the Nevada Test Site are silicates, although there is some dolomite. Specifically, the material used in the HCTF is either silica or alumina. Silicon and aluminum have similar, but not identical, neutron transport properties. We therefore used Monte Carlo calculations similar to those used in our original studies (Hearst, 1974) to learn the effect of different materials. At most combinations of density and water content studied, the change in apparent I_H is less than 0.01. At one value it might be as much as 0.03, but this is likely an artifact of the statistics of the specific Monte Carlo calculation. This difference in materials is, of course, one of the differences between our calibration and the contractor's, and its effect is included in the section on hole shape.

In summary, the most important imperfections in the calibration facility are the floor and the shape of the hole, and they produce uncertainties of unknown size for some cases. Hole size and shape effects will be reduced by shielding, especially to the big-hole sonde.

However, there are fluctuations in the measurements at different heights that cannot be attributed to specific imperfections. If their effect persists when the shielding is added to the big-hole sonde, these effects will have to be included in the differences used to calculate $\sigma^2(i)$.

IMPERFECTIONS IN THE WORLD

The discussion above has assumed the medium outside the hole to be homogeneous and isotropic. Usually it is not. We can approximate an inhomogeneous or anisotropic situation by assuming: (1) the medium consists of two materials, and (2) the path from source to detector is made up of these

materials in series or in parallel. In the development of the algorithm (Appendix) we let

$$N_N = C \exp(-r/\lambda_{tr}) \quad , \tag{17}$$

and

$$\lambda_{tr} = v(\rho) \exp w(I_H) \quad . \tag{18}$$

If n materials, each having a thickness that is a fraction f_i of the total, are in series, then

$$N_N = C \exp\left[-\sum_{i=1}^{n} \frac{rf_i}{n}/v(\rho_i) \exp w(I_{Hi})\right] . \tag{19}$$

If in parallel, with an angular extent f_i of the total angular extent,

$$N_N = \frac{C}{n}\sum \exp\left[-rf_i/v(\rho_i) \exp w(I_{Hi})\right] \tag{20}$$

We calculated the apparent water content from N_N for series and parallel cases for n = 2 and compared it to the mean water content. We did a series of calculations for mean values of 0.1, 0.2, 0.3 and upwards, letting I_{H1} vary from 10 to 90% of the mean and f_1 vary from 0.1 to 0.9. We calculated I_{H2} from I_{H1}, f_1, and the mean. The apparent water is always lower than the mean and always lower for parallel than series. As an example, for equal volumes of I_{H1} = 0.1 and I_{H2} = 0.3, the mean is 0.2. The apparent water for series is 0.186 and for parallel 0.169. Some typical curves are shown in Fig. 11.

We have concluded that this is an uncertainty that is plausible in a medium made up of a matrix with boulders that are drier than the matrix and might give errors as large as 0.025.

DATA REDUCTION PROCEDURE

After a neutron log has been run, it is digitized--either in the field or from the paper log. The log is normally recorded in API units, because the company's environmental calibrator gives a conversion from counts to API units

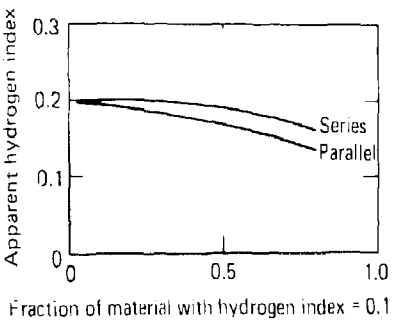

FIG. 11. Apparent water content in an inhomogeneous medium. Mean water content is 0.2; one material has a water content of 0.1. Apparent water content plotted vs fraction of that material for series and parallel situations.

at three values of count, and this accounts for day-to-day variations in the logging system. The gap record and a density log are also digitized. All three digital records are smoothed to give a 20-s running average of each of the three variables. (Depth is adjusted as required.) Then a root-finder with constants a_1-a_5 appropriate to the specific sonde is used to find I_H from N_N, ρ, and G. (Each sonde must be calibrated separately.) Because our users demand a log of weight-fraction water, all values of I_H are divided by the appropriate value of ρ, to give a final log of weight-fraction water vs depth.

Figure 12 shows an original log and the corresponding final log. The latter is compared to sample data. These samples were obtained with a Hunt sidewall sampler mounted on the drill string. They were first heated to 105 C, and the weight loss measured, then heated to 700 C and the evolved hydrogen measured. This procedure obtained the total weight-fraction water (or water equivalent if bound hydrogen is not all in the form of water).

There is some doubt that these sample data represent the true water content at it is observed by the log. First, the sidewall sampler often simply scr ; the wall of the large-diam hole rather than going into the wall; ..wise, it penetrates only about 8 cm. This means that the sample can easily be contaminated with drilling fluid to a much greater extent than the volume seen by the log. Also, because the hole is so large, it is quite likely that the sample is taken from a different part of the hole than the

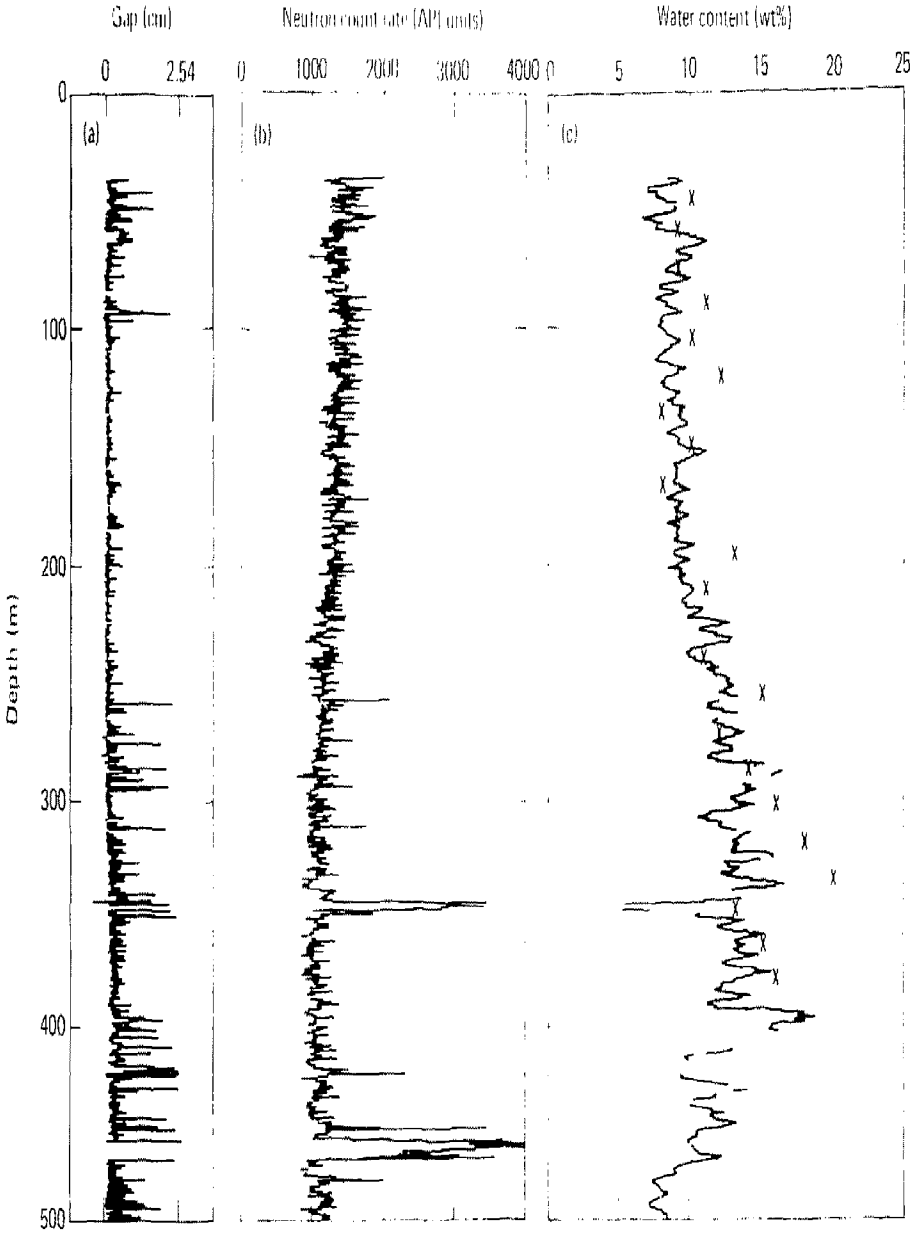

FIG. 12. Raw gap (a), count (b) and final log (c) in a 2.5-m hole at the Nevada Test Site. The x's on 12(c) are sample data taken at 700°.

r, possibly 1 or 2 meters from the logged point. In alluvium, water content can vary markedly over a meter or two horizontally, and often boulders are present.

The log shown was obtained with the small sonde (with its inadequate shield), and we have not yet developed a satisfactory hole-size correction. So it is likely that at a weight-fraction water of 0.125, the weight fractions are low by about 0.03. (See discussion of hole-size effects above.) Because there is only one gap-measuring wheel on that sonde, a large gap uncertainty still exists.

The log appears to agree with the lowest values of the sampled water content. This type of agreement is typical of our comparisons of logs and sample data. We think that this tracking of the low values occurs because drilling fluid invasion gives spuriously high sample water contents near the borehole. We have considerable evidence that fluid invasion does indeed take place and affects the density near the borehole (Hearst, et al, 1968).

We have found a substantial lack of correlation between neutron-log readings and sample data in alluvium and tuff (Hearst, 1974b). However, we have not at this writing been able to demonstrate the connection between this information and the lack of agreement between water contents calculated from our algorithm and the sample data. Another possibility that cannot be dismissed is that the neutron log--with our method of data reduction--is, in fact, useless for determining water content at the NTS.

CONCLUSION

There are many sources of uncertainty in the estimate of water content from a neutron log. We believe we have minimized the effects of imperfections in the calibration facility by design of the facility and compensation in the calibration algorithm. (It should be realized that the circuitry in the ordinary neutron log panel is such an algorithm.) Some imperfections in the measurement, such as hole size, can be corrected also.

Inhomogeneity in the world produces uncertainties that cannot be eliminated. The log analyst may be able to estimate its effect, and, since he knows its direction, he may be able to compensate for it.

The remaining sources--in our case lack of fit in the algorithm and uncertainty in both gap and count--cannot be eliminated, only recognized. If we sum the bias shown in Figs. 7 or 8, and the effect of measurement uncertainty shown in Fig. 6, we find the total uncertainty to be the larger of 8% of the hydrogen index or 0.02 for the big-hole sonde (at values up to 0.5) for plausible values of uncertainties in gap and count. If we take into account the effects of differences in measurement height, the total uncertainty with a small sonde can increase up to 11%. We have not tested this with a big-hole sonde.

Work remains to be done. The big-hole sonde must be recalibrated after shielding has been added. At that time we will be able to learn if the variations of count with position on the cells are significant. If so, these variations must be included in the uncertainty of the final calibration of the big-hole sonde.

ACKNOWLEDGMENTS

We wish to thank D. Chakedis and his crew and W. McKinnis for their assistance in modifying the test facility. R. Cothron, R. Smith, and R. Fenster were in charge of the logging crews who took the data. S. Clark was a great help, both in taking and analyzing the data.

APPENDIX

We can justify the form that we chose as follows: The diffusion of neutrons is governed by the Boltzmann equation (describing the conservation of neutrons). Under simplifying assumptions (e.g., no neutron capture) the stationary-state Boltzmann equation can be reduced to either the single-velocity elementary diffusion equation or the age equation (Morrison and Feld, 1953). We can further simplify the conditions for the age equation, and consider a point source of Q neutrons per second of energy E_0 in a homogeneous, hydrogenous, slowing-down medium that is infinite. In this case the solution of the age equation at some radial position r from the source is approximated by

$$q(r,E_0') = \left(\frac{Q}{4\pi\lambda_{tr}(E_0)r^2}\right) \exp\left[-r/\lambda_{tr}(E_0)\right] \quad \text{(Morrison and Feld, 1953)} \qquad (21)$$

The "slowing-down density" $q(r,E_0')$ represents the rate at which neutrons (in unit volume and unit logarithmic energy E) pass through the energy $E_0' = E_0/e$, and λ_{tr} is the transport mean free path for scattering the neutron until it is captured or thermalized (and therefore no longer available to an epithermal detector).

The neutron density function (neutrons/cm^3) for neutrons of a given energy E, velocity v, and scattering mean free path λ_{sc} is

$$n(r,E) = \frac{\lambda_{sc}(E)}{\xi v(E)}\, q(r,E) \quad , \qquad (22)$$

since neutrons of energy E make v/λ_{sc} collisions per unit time and lose on the average the logarithmic energy ξ per collision. The neutron count rate at energy E and radius r from the source can be approximated by

$$N_N \frac{\text{Neutrons}}{s} \approx n(r,E)\, 4\pi r^2\, v(E) = \frac{\text{Const.}\ \lambda_{sc}}{\xi\lambda_{tr}} \exp\left(-r/\lambda_{tr}\right) \quad . \qquad (23)$$

(The solution to the diffusion equation for a point source can be approximated by a similar expression with λ_{tr} replaced by $\sqrt{\lambda_{tr}\lambda_a}$, where λ_a is the absorption cross section.) With increasing water content, the average

logarithmic energy loss per collision ξ increases, while λ_{tr} and λ_{sc} decrease. However, λ_{tr} decreases much more rapidly than λ_{sc}, so the coefficient of the exponential is a slowly varying function of water content. We have chosen to approximate it by a constant. If we also assume N_N is independent of energy, we have

$$N_N = \text{Const.} \exp\left(-r/\lambda_{tr}\right) . \tag{24}$$

Kozkevnikov's (1963) calculated curves of the slowing-down length L_s vs porosity suggest an exponential decrease of L_s with increasing porosity and, therefore, water content (assuming 100% saturation). We now arbitrarily assume that $\lambda_{tr} \propto L_s$ and can be represented by an equation of the form

$$\lambda_{tr} = V(\rho) \exp\left[W(I_H)\right] , \tag{25}$$

where $V(\rho)$ and $W(I_H)$ are functions of bulk density and hydrogen index, respectively. Taking logarithms to simplify the final equation results in

$$\ln N_N = C + V(\rho) \exp\left[W(I_H)\right] . \tag{26}$$

Trial functions for $V(\rho)$ and $W(I_H)$ were chosen by visually inspecting the plotted calibration data.

At this point it is necessary that we remind ourselves of the idealized nature of this equation. We have not considered neutron capture or inelastic scattering. We have assumed radial neutron flow in an infinite, homogenous, isotropic medium; we have assumed energy independence, and finally, we have assumed a perfectly absorbing detector.

REFERENCES

Allen, L. S., W. R. Mills, K. P. Desai, and R. L. Caldwell, 1972, Some Features of Dual-Spaced Neutron Porosity Logging, Trans. Soc. Prof. Well Log Analysts, 13th Annual Logging Symposium, Tulsa, May 7-10, Paper G.

Delhomme, J. F., 1978, Kriging in the Hydrosciences, Advanced in Water Resources, v. 1, No. 5, pp. 251-266.

Diment, W. H., 1959, Trace Element Memoranda, Nos. 996, 997, and 998, U. S. Geological Survey, Washington, D.C.

Hearst, J. R, 1979, Calibration of a Neutron Log in Partially Saturated Media, Trans. Soc. Prof. Well Log Analysts, 20th Annual Logging Symposium, Tulsa, June 3-6, Paper B.

Hearst, J. R, 1974, Effects of Bulk Density on Calculated Neutron Log Response, Nuc. Inst. and Methods, v. 117, p. 141.

Hearst, J. R, 1974b, On the Comparison of the Data From an Epithermal Neutron Log to Water Content Measured From In Situ Samples in Yucca Flat, Nevada Test Site, Lawrence Livermore National Laboratory, Livermore, Calif., UCID-16475.

Hearst, J.R, V. E. Wheeler, and J. T. Rambo, 1968, On the Effect of Drilling Fluid on Measured Density in Alluvium, Lawrence Livermore National Laboratory, Livermore, Calif., UCID-15313.

International Mathematical Statistical Library, Inc. (IMSL), 1978, Minimum of the Sum of Squares of M Functions in N Variables Using a Finite Difference Levenberg-Maquardt Algorithm, Code ZXSSQ8.

Kozhevnikov, D. A., 1963, Calculation of the Neutron Characteristics of Rocks, Trudy Moskov. Inst. Neft. i Gazovio Prom., No. 14, pp. 54-75. Translated from the Russian (January 1967) by ?. F. St. Gallay.

Morrison, P. and B. T. Feld, 1953, Experimental Nuclear Physics, Vol. II, E. Segre (Editor), John Wiley & Sons, Inc., New York.

Segesman, F. and O. Liu, 1971, The Excavation Effect, Trans. Soc. Prof. Well Log Analysts, 12th Annual Logging Symposium, Dallas, May 2-5, Paper N.

Tittle, C. W., 1961, Theory of Neutron Logging, I, Geophysics, v. 26, No. 1, p. 27.

Tittman, J. et al., 1966, The Sidewall Epithermal Neutron Porosity Log, J. Petr. Tech., v. 18, p. 1351.

NOMENCLATURE

a_1, a_2, a_3, a_4	Coefficients obtained by fitting zero-gap data.
a_5	Coefficient of the gap term in the fit.
C	A constant.
e_G, e_N, e_ρ	Errors in the measurement of gap, count, and density, respectively.
e(i)	One of the errors in m measurements of count rate in a calibration set.
E_0, E_0'	Initial neutron energy and that energy divided by 2.7183 2.7183 (e).
f_i	Fractions of material of different water content in a mixture.
F	"True" form of function describing water content in terms of count rate, density, and gap.
G	Gap between sonde and borehole wall.
G_K	Observed value of gap in a borehole.
G(i)	One of m measurements of gap in a calibration set.
H	Fitted form of function describing water content in terms of count rate, density, and gap.
i	Index of measurements in a calibration set.
I_H	Hydrogen index: Hydrogen content per unit volume compared to that in fresh water.
$\hat{I}_H$	Estimated value of I_H.
j	Index of calibrations under different borehole or sonde configurations.
L_s	Neutron "slowing-down length."
m	Number of points in a calibration set (11 normally).
M	Conversion factor from counts/s to API units.
n(r,E)	Number of neutrons of energy E at radius r per cubic cm.
N_N	Neutron count rate in API units.
N_N'	Neutron count rate in counts/s.
$N_N^0(i)$	True neutron count rate for one of the m calibration sets.
$N_N(i)$	Observed neutron count rate in one of the m calibration sets.
N_{NK}	Observed neutron count rate in a borehole.

$\bar{N}_N$	Neutron count rate that would be observed during a very long count in an infinite homogeneous medium.
N_N	Vector of the $N_N(i)$.
$\overline{q(r,E)}$	Rate at which neutrons pass through energy E at radius r (the slowing-down density).
Q	Neutron source strength (neutrons/s).
r	Radius from the neutron source.
U	Arbitrary function.
v(E)	Neutron velocity.
$v(\rho), V(\rho)$	Functions of the density.
$w(I_H), W(I_H)$	Functions of the hydrogen index.
y	Logarithm of X, the neutron count rate.
$\hat{y}$	Estimate of y.
$\epsilon I(cal)$	Zero-mean, random variable describing the uncertainty in I_H caused by measurement uncertainties in the calibration.
$\epsilon I(data)$	Zero-mean, random variable describing the uncertainty in I_H caused by measurement uncertainties in the borehole.
$\epsilon I(fit)$	Uncertainty in I_H caused by bias in the calibration.
ϵI	Total uncertainty in I_H: I(cal) + I(data) + I(fit).
ξ	Logarithm of neutron energy.
$\lambda_a, \lambda_{sc}, \lambda_{tr}$	Absorption, scattering, and transport mean free path.
ξ_0	Logarithmic energy loss per collision.
ρ	Bulk density.
ρ_K	Observed value of bulk density in a borehole.
$\rho(i)$	One of m measurements of bulk density in a calibration set.
$\sigma^2(i)$	Variance of e(i), the errors of measured count rate in the calibration.
$\sigma_G^2, \sigma_{N_N}^2, \sigma_\rho^2$	Variances of errors in the gap, count rate, and density in a borehole.
$\sigma_{N_N}^2$ (exp)	Part of variance in N_N not caused by statistical fluctuations.
σ_y^2(exp)	Part of variance of ln (N_N) not caused by statistical fluctuations.

CG/ks

Hearst

Kasameyer

Joseph R Hearst received a B.A. degree in Physics from Reed College, followed by a B.S. in Business and Engineering Administration from Massachusetts Institute of Technology in 1954, an M.A. in Physics from Boston University in 1955, and a Ph.D. from Northwestern University in 1959.

He then joined Lawrence Livermore National Laboratory of the University of California and in 1963 became a member of the Earth Sciences Division of that Laboratory. He is at present a member of the Applied Geophysics Group.

In recent years his work has been in two major fields: rock mechanics and borehole geophysics. In the former he has studied the effects of contained explosions, both nuclear and conventional, on earth materials. For some time he concentrated on explosive-induced fracturing and was Project Scientist for the Kemmerer Coal Outcrop Fracture Experiment in 1974. In the latter field he has worked on well-logging in non-standard conditions and has published work on high-resolution seismic surveys, dry-hole acoustic logging, density, and neutron logging and borehole gravimetry.

From March to September 1979, Dr. Hearst was a Senior Fulbright Research Scholar at the University of Queensland, Brisbane, Australia.

Paul W. Kasameyer is the leader of the Applied Geophysics Group at Lawrence Livermore National Laboratory. He graduated from the Massachusetts Institute of Technology (MIT) in 1965, earned an M.A. in physics at Yale, and returned to MIT to receive his Ph.D. in geophysics in 1974. He has published work in the areas of heat flow, magnetotellurics, geothermal modeling, and in situ measurements.

Dreiling

Leslie A. Dreiling was born May 10, 1946 in Hays, Kansas. He received a B.S. degree in physics from Fort Hays State University in 1968 and an M.S. degree in physics from Kansas State University in 1970. In 1976, he received a Ph.D. in astronomy from the University of Maryland, College Park.

From 1970 to 1972 he worked as an associate physicist at the Johns Hopkins University Applied Physics Laboratory, Howard County, Md. In 1976 he joined the Lawrence Livermore National Laboratory as a computational physicist.

Dr. Dreiling is a member of Phi Kappa Phi and the American Astronomical Society.